Available online at www.sciencedirect.com
SCIENCE DIRECT®
International Journal of Heat and Mass Transfer 47 (2004) 1889–1905
International Journal of HEAT and MASS TRANSFER
www.elsevier.com/locate/ijhmt

Analysis of flow and heat transfer in porous media imbedded inside various-shaped ducts

A. Haji-Sheikh [a,*], K. Vafai [b]

[a] Department of Mechanical and Aerospace Engineering, The University of Texas at Arlington, 500 West First Street, Arlington, TX 76019-0023, USA

[b] Department of Mechanical Engineering, University of California, Riverside, CA 92521-0425, USA

Received 23 July 2003; received in revised form 20 October 2003

Abstract

Heat transfer to a fluid passing through a channel filled with porous materials is the subject of this investigation. It includes the derivation of the temperature solutions in channels having different cross sectional geometries. Primarily, consideration is given to a modified Graetz problem in parallel plate channels and circular tubes. This presentation includes numerical features of the exact series solution for these two ducts using the Brinkman's model. The results are compared to results from another numerical study based on the method of weighted residuals. Moreover, as a test case, the method of weighted residuals provided flow and heat transfer in elliptical passages. The results include the computation of heat transfer to fluid flowing through elliptical passages with different aspect ratios.

1. Introduction

In many applications, the Darcy's law is inapplicable where the fluids flow in porous media bounded by an impermeable boundary. For these cases, the study of convective heat transfer should include inertia and boundary effects. A number of recent studies incorporated these effects by using the general flow model known as the Brinkman–Forschheimer-extended Darcy model. For example, Kaviany [1] used the Brinkman-extended Darcy model to obtain a numerical solution of laminar flow in a porous channel bounded by isothermal parallel plates. Vafai and Kim [2], using this model, studied forced convection for thermally fully developed flow between flat plates while Amiri and Vafai [3] reported a numerical study on the thermally developing condition. Also, for flow in parallel plate channels, Lee and Vafai [4] used a two-equation model to study the effect of local thermal non-equilibrium condition. Alazmi and Vafai [5] extended the earlier work by investigating different porous media transport models.

An extensive study of flow in porous media is available in [6–8]. Angirasa [9] discusses the history of development of transport equations in porous media and finite difference simulations. Nield et al. [10] presented the effect of local thermal non-equilibrium on thermally developing forced convection in a porous medium. These references are valuable in this investigation of the accuracy and utility of the exact series solution presented here. The exact series solution requires the computation of a set of eigenvalues and the numerical computation of certain eigenvalues can become a formidable task. In practice, using, e.g., a 32 bit-processor, it may not be possible to compute a large number of eigenvalues. To verify the accuracy of the series solution, the use of an alternative method of analysis becomes necessary. The closed-form solution that uses the method of weighted residuals is selected. It provides solutions with comparable accuracy over an extended range of variables. For a finite number of eigenvalues, the method of weighted residuals provides results with comparable accuracy at larger values of the axial coordinate. Because it is based on variational calculus and the minimization principle, it yields

* Corresponding author. Tel.: +1-817-272-2010; fax: +1-817-272-2952.
E-mail address: haji@mae.uta.edu (A. Haji-Sheikh).

0017-9310/$ - see front matter © 2003 Elsevier Ltd. All rights reserved.
doi:10.1016/j.ijheatmasstransfer.2003.09.030

Nomenclature

A	area, m^2
$\mathbf{A}$	matrix
A_m, a_i	coefficients
a	elliptical duct dimension, m
a_{ij}	elements of matrix $\mathbf{A}$
B_m	coefficient
$\mathbf{B}$	matrix
b	elliptical duct dimension, m
b_{ij}	elements of matrix $\mathbf{B}$
C	duct contour, m
c_n	coefficients
c_p	specific heat, J/kg K
$\mathbf{D}$	matrix
Da	Darcy number, K/L_c^2
D_h	hydraulic diameter, m
d_{mj}	elements of matrix $\mathbf{D}$
d_n	coefficients
F	pressure coefficient
f	Moody friction factor
h	heat transfer coefficient, $W/m^2 K$
$\bar{h}$	average heat transfer coefficient, $W/m^2 K$
i, j	indices
K	permeability, m^2
k	effective thermal conductivity
L_c	characteristic length
M	μ_e/μ
N	matrix dimension
Nu_D	Nusselt numbed hD_e/k
m, n	indices
$\mathbf{P}$	matrix having elements p_{mi}
Pe	Peclet number, $\rho c_p L_c U/k$
p	pressure, Pa
p_{mi}	elements of matrix $\mathbf{P}$
r	radial coordinate
r_o	pipe radius, m
S	volumetric heat source, W/m^3
T	temperature, K
T_i	temperature at $x = 0$, K
T_w	wall temperature, K
u	velocity, m/s
$\bar{u}$	$\bar{u} = \mu u/(\Phi L_c^2)$
U	average velocity, m/s
$\overline{U}$	average value of $\bar{u}$
x	axial coordinate, m
$\bar{x}$	$x/(PeH)$ or $\bar{x} = x/(Per_o)$
y, z	coordinates, m

Greek symbols

β	coefficient, Eqs. (16b) or (46a)
Φ	$-\partial p/\partial x$
λ_m	eigenvalues
μ	viscosity coefficient, N s/m^2
θ	$(T - T_w)/(T_i - T_w)$
μ	fluid viscosity
μ_e	effective viscosity, N s/m^2
ψ	coefficient, Eq. (16a) or (46b)
ξ	dimensionless coordinate
ρ	density, kg/m^3
η	y/H or r/r_o
ω	parameter, $\sqrt{M\,Da}$

significantly higher accuracy near the thermal entrance region. In addition, standard-computing packages can produce all eigenvalues with ease instead of getting them one at a time.

In summary, the presentation in this paper begins by providing the exact mathematical solution for heat transfer in the entrance region of a parallel plate channel. The procedure is then extended to compute similar parameters in a circular duct. Here, the eigenfunctions for both cases are obtained analytically. Later, an alternative solution technique that uses the method of weighted residuals [11] is used to reproduce the information gathered for parallel plate channels and circular ducts. A unique feature of this method is its ability to accommodate flow passages having various cross sectional profiles. To demonstrate the utility of this alternative solution method, information concerning developing heat transfer in the entrance region of various elliptical ducts is also reported here.

2. General formulation of velocity and temperature

Heat transfer to a fully developed flow though a porous media confined within an impermeable wall is of interest in this study. This paper considers heat transfer in parallel plate channels, circular pipes, and elliptical passages in the absence of any volumetric heat source and axial heat conduction. The Brinkman momentum equation for a fully developed flow is

$$\mu_e \nabla^2 u - \frac{\mu}{K} u - \frac{\partial p}{\partial x} = 0. \tag{1}$$

Here, fluid flows in the direction of x and the Laplace operator takes different forms depending on the shape of the passages. The energy equation in its reduced form is

$$u \frac{\partial T}{\partial x} = \frac{k}{\rho c_p} \nabla^2 T + \frac{1}{\rho c_p} S, \tag{2}$$

where S is the classical volumetric heat source that includes the contribution of frictional heating. Various theories concerning the form of S are in Nield et al. [12,13]. For the three specific cases presented in this study, it is assumed that there is no frictional heating, $S = 0$. Eqs. (1) and (2) in conjunction with the given wall and entrance conditions provide velocity and temperature fields. The energy balance on a differential fluid element produces the relation $hC(T_w - T_b) = \rho UA(dT_b/dx)$ where U is the average velocity, C is the contour of the duct, A is the passage area, T_w is the constant wall temperature, and $T_b = T_b(x)$ is the local bulk or mean temperature of the fluid defined as

$$T_b = \frac{1}{A}\int_A \left(\frac{u}{U}\right) T\, dA. \tag{3}$$

Let L_c be a characteristic length selected depending the shape of a passage and U to designate the average fluid velocity in the passage. As an example, for a circular pipe, $L_c = r_o$ where r_o is the pipe radius. This produces the working relation for computing the dimensionless local heat transfer coefficient hL_c/k as

$$\frac{hL_c}{k} = \left(\frac{\overline{A}}{\overline{\overline{C}}}\right)\left[\frac{dT_b(\bar{x})/d\bar{x}}{T_w - T_b(\bar{x})}\right] = -\left(\frac{\overline{A}}{\overline{\overline{C}}}\right)\left[\frac{d\theta_b(\bar{x})/d\bar{x}}{\theta_b(\bar{x})}\right], \tag{4a}$$

where $\bar{x} = x/(PeL_c)$, $Pe = \rho c_p L_c U/k$, $\overline{A} = A/L_c^2$, $\overline{C} = C/L_c$, and assuming $T_b(0) = T_i$ to be a constant makes $\theta_b(x) = [T_b(\bar{x}) - T_w]/(T_i - T_w)$. This equation yields the standard definition of the Nusselt number $Nu_D = hD_h/k$, based on the hydraulic diameter $D_h = 4A/C$, as

$$\frac{hD_h}{k} = -\left(\frac{D_h^2}{4L_c^2}\right)\left[\frac{d\theta_b(\bar{x})/d\bar{x}}{\theta_b(\bar{x})}\right]. \tag{4b}$$

Using the definition of the average heat transfer coefficient,

$$\bar{h} = \frac{1}{x}\int_0^x h\, dx, \tag{5a}$$

Eqs. (4a) and (4b) yield

$$\frac{\bar{h}L_c}{k} = -\left(\frac{\overline{A}}{\overline{\overline{C}}}\right)\left[\frac{\ln\theta_b(\bar{x})}{\bar{x}}\right] \tag{5b}$$

and

$$\frac{\bar{h}D_h}{k} = \left(\frac{D_h^2}{4L_c^2}\right)\left[\frac{\ln\theta_b(\bar{x})}{\bar{x}}\right]. \tag{5c}$$

The subsequent analyses report the results using these four definitions of the dimensionless heat transfer coefficients.

3. Velocity and temperature fields in parallel plate channels

The first flow model considers a steady and hydrodynamically fully developed flow between two impermeable parallel plates, $2H$ apart (see Fig. 1). The computation begins by considering the Brinkman momentum equation

$$\mu_e\frac{\partial^2 u}{\partial y^2} - \frac{\mu}{K}u - \frac{\partial p}{\partial x} = 0. \tag{6a}$$

Assuming constant pressure gradient $\Phi = -\partial p/\partial x$ and using the effective viscosity μ_e, the fluid viscosity μ, the permeability K, and $L_c = H$, Eq. (6a), in dimensionless form, reduces to an ordinary differential equation

$$M\frac{d\bar{u}}{d\bar{y}} - \frac{1}{Da}\bar{u} + 1 = 0, \tag{6b}$$

where $\bar{y} = y/H$, $M = \mu_e/\mu$, $\bar{u} = \mu u/(\Phi H^2)$, and $Da = K/H^2$ is the Darcy number. The solution of Eq. (6b) using the boundary conditions $\bar{u} = 0$ at $\bar{y} = 1$ and the symmetry condition $\partial\bar{u}/\partial\bar{y} = 0$ at $\bar{y} = 0$ becomes

$$\bar{u} = Da\left[1 - \frac{\cosh(\omega\bar{y})}{\cosh(\omega)}\right], \tag{7}$$

where $\omega = (MDa)^{-1/2}$. Then, using the mean velocity defined by the relation

$$U = \frac{1}{H}\int_0^H u\, dy. \tag{8}$$

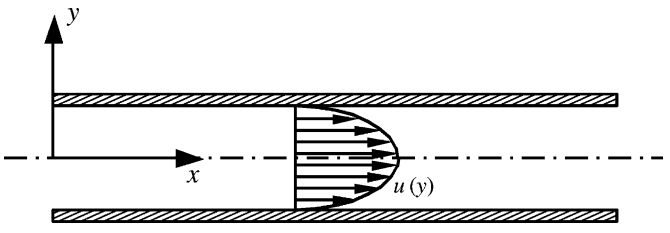

Fig. 1. Schematic of a flow in a parallel plate channel.

Eq. (7) leads to a relation for the reduced mean velocity $\overline{U}$ as,

$$\overline{U} = Da[1 - \tanh(\omega)/\omega], \tag{9a}$$

and therefore

$$\frac{u}{U} = \frac{\bar{u}}{\overline{U}} = \frac{\omega}{\omega - \tanh(\omega)}\left[1 - \frac{\cosh(\omega\bar{y})}{\cosh(\omega)}\right]. \tag{9b}$$

The definition of the average velocity $\overline{U} = \mu U/(\Phi H^2)$ leads to a relation for the friction factor

$$f = -\frac{(\partial p/\partial x)D_h}{\rho U^2/2} = \frac{2}{\overline{U}}\frac{1}{Re_D}\left(\frac{D_h}{H}\right)^2 = \frac{F}{Re_D}, \tag{10}$$

where $F = (2/\overline{U})(D_h/H)^2$. Moreover, Eq. (8) provides the value of $\overline{U}$ once the function $\bar{u}$ replaces u in the integrand.

The temperature distribution assuming local thermal equilibrium is obtainable from the energy equation

$$u\frac{\partial T}{\partial x} = \frac{k}{\rho c_p}\frac{\partial^2 T}{\partial y^2}. \tag{11a}$$

Introducing the Peclet number $Pe = \rho c_p HU/k$ where U is the mean velocity in the duct, and dimensionless $\bar{x} = x/(PeH)$, the energy equation (Eq. (11)) reduces to

$$\frac{u}{U}\frac{\partial\theta}{\partial\bar{x}} = \frac{d^2\theta}{d\bar{y}^2}, \tag{11b}$$

where θ is the dimensionless temperature $\theta = (T - T_w)/(T_i - T_w)$. In this formulation, it is assumed that the inlet temperature T_i and the wall temperature T_w have constant values.

The solution of the partial differential Eq. (11b) is obtainable using the method of separation of variables; that is, let $\theta(\bar{x},\bar{y}) = X(\bar{x})Y(\bar{y})$. The substitution of this functional for θ in Eq. (11b) yields

$$\frac{u}{U}\frac{X'}{X} = \frac{Y''}{Y} \tag{12}$$

leading to two ordinary differential equations

$$X'(\bar{x}) + \lambda^2 X(\bar{x}) = 0 \tag{13a}$$

and

$$Y''(\bar{y}) + \lambda^2\left(\frac{u}{U}\right)Y(\bar{y}) = 0. \tag{13b}$$

The parameter λ is the eigenvalue in this eigenvalue problem that produces the temperature solution

$$\theta = \sum_{m=1}^{\infty} B_m Y_m(\bar{y})e^{-\lambda_m^2\bar{x}}, \tag{14}$$

where the term $e^{-\lambda_m^2\bar{x}}$ in Eq. (14) is the solution of Eq. (13a) once the parameter λ is replaced by λ_m. However, the solution of Eq. (13b) remains as the major task for this investigation and it is presented in the following sections.

Following substitution for u/U, Eq. (13b) takes the following form:

$$Y''(\bar{y}) + \lambda^2\left\{\frac{\omega}{\omega - \tanh(\omega)}\left[1 - \frac{\cosh(\omega\bar{y})}{\cosh(\omega)}\right]\right\}Y(\bar{y}) = 0. \tag{15}$$

Next, consideration is given to the exact and numerical solutions of this ordinary differential equation. For simplicity of this presentation, let

$$\psi = \frac{\lambda^2/\omega}{\omega - \tanh(\omega)} \tag{16a}$$

and

$$\beta = \frac{1}{\cosh(\omega)}, \tag{16b}$$

then Eq. (15) reduces to

$$Y''(\bar{y}) + \omega^2\psi[1 - \beta\cosh(\omega\bar{y})]Y(\bar{y}) = 0. \tag{17}$$

This differential equation has the form of a modified Mathieu differential equation whose solution is associated with the modified Mathieu Function [14]. Various classical solutions of the Mathieu differential equation are in [14,15]. However, the plus sign instead of a minus sign in Eq. (17) makes its solution more demanding than the classical modified Mathieu Function. Since this is a special Mathieu differential equation, it is best to describe the method of solution for this special case. Among a few possible solutions, two different solutions are presented here.

First solution: For convenience of algebra, the abbreviated form of this ordinary differential equation is

$$Y'' + \omega^2\psi[1 - \beta\cosh(\omega\bar{y})]Y = 0, \tag{18}$$

where $\psi = (\lambda^2/\omega)/[\omega - \tanh(\omega)]$ and $\beta = 1/\cosh(\omega)$. The boundary conditions require having a symmetric condition at $y = 0$ and $Y = 0$ at $y = H$ or $\bar{y} = 1$; they are $Y'(0) = Y(1) = 0$. For convenience of algebra, using a new independent variable $\eta = \cosh(\omega\bar{y}) - 1$, one obtains

$$\frac{dY}{d\bar{y}} = \frac{dY}{d\eta}\frac{d\eta}{d\bar{y}} = \frac{dY}{d\eta}[\omega\sinh(\omega\bar{y})] \tag{19}$$

and

$$\begin{aligned}\frac{d^2Y}{d\bar{y}^2} &= \frac{d^2Y}{d\eta^2}[\omega\sinh(\omega\bar{y})]^2 + \frac{dY}{d\eta}[\omega^2\cosh(\omega\bar{y})]\\ &= \omega^2\sinh^2(\omega\bar{y})\frac{d^2Y}{d\eta^2} + \omega^2\cosh(\omega\bar{y})\frac{dY}{d\eta}\\ &= \omega^2[(\eta+1)^2 - 1]\frac{d^2Y}{d\eta^2} + \omega^2(1+\eta)\frac{dY}{d\eta}.\end{aligned} \tag{20}$$

Following appropriate substitution, the resulting differential equation is

$$(\eta^2+2\eta)\frac{d^2Y}{d\eta^2}+(\eta+1)\frac{dY}{d\eta}+\psi(1-\beta-\beta\eta)Y=0. \quad (21)$$

It is interesting to note that the boundary conditions $dY/dy=0$ when $y=0$ or $\eta=0$ is automatically satisfied regardless of the value of $dY/d\eta$. The solution of this differential equation is a hypergeometric function and two different solutions are in the following sections.

To obtain this solution by a standard technique, let

$$Y(\eta)=\sum_{n=0}^{\infty}c_n\eta^n, \quad (22a)$$

and then differentiate to get

$$\frac{dY(\eta)}{d\eta}=\sum_{n=0}^{\infty}c_n n\eta^{n-1} \quad \text{for } n>0 \quad (22b)$$

and

$$\frac{d^2Y(\eta)}{d\eta^2}=\sum_{n=0}^{\infty}c_n n(n-1)\eta^{n-2} \quad \text{for } n>1. \quad (22c)$$

The substitution for $Y(\eta)$ and its derivatives in the differential equation (Eq. (21)) produces

$$\sum_{n=2}^{\infty}c_n n(n-1)(\eta^n+2\eta^{n-1})+\sum_{n=1}^{\infty}c_n n(\eta^n+\eta^{n-1}) + \sum_{n=0}^{\infty}c_n\psi[(1-\beta)\eta^n-\beta\eta^{n+1}]=0. \quad (23)$$

The examination of Eq. (22) shows that c_0 is a constant since $Y(0)\neq 0$. This leads to the condition that $dY/d\eta\neq 0$ when $\eta=0$ or $c_1\neq 0$. Therefore, in the above equation, the terms that contain the parameter η^0 take the following form:

$$c_1\cdot 1\cdot\eta^0+c_0\psi(1-\beta)\eta^0=0 \quad (24a)$$

which makes $c_1+c_0\psi(1-\beta)=0$ or $c_1=-c_0\psi(1-\beta)$. Next, the examination of the coefficients that multiply by η^1 shows that

$$[4c_2+c_1+2c_2+c_1\psi(1-\beta)-c_0\psi\beta]\eta^1=0. \quad (24b)$$

This procedure is to be repeated for η values with exponents $2,3,\ldots$ and so on. In general, the examination of the coefficients that multiply η^{n-1} leads to the relation

$$[(n-1)(n-2)c_{n-1}+2n(n-1)c_n+(n-1)c_{n-1} + nc_n+\psi(1-\beta)c_{n-1}-\psi\beta c_{n-2}]\eta^{n-1}=0. \quad (24c)$$

Since $\eta\neq 0$, then the solution for c_n is

$$c_n=-\frac{n^2-2n-n+2+n-1+\psi(1-\beta)}{2n^2-2n-n}c_{n-1} + \frac{\psi\beta}{2n^2-2n-n}c_{n-2} = -\frac{(n-1)^2+\psi(1-\beta)}{n(2n-1)}c_{n-1}+\frac{\psi\beta}{n(2n-1)}c_{n-2}. \quad (24d)$$

In summary, the solution can be rewritten as

$$Y(\bar{y})=1+\sum_{n=1}^{\infty}c_n\Big[\cosh(\omega\bar{y})-1\Big]^n. \quad (25)$$

In this formulation, $c_0=1$ is selected arbitrarily, then $c_1=-c_0\psi(1-\beta)$ and the recursive relation (24d) provide the remaining coefficients c_n for $n\geqslant 2$. It should be noted that there are other possible variations of this solution, e.g., $\eta=\beta\cosh(\omega y)$, $\eta=[1-\cosh(\omega\bar{y})]/\cosh(\omega)$ with $0\leqslant\eta\leqslant 1$.

Second solution: As an alternative solution of this ordinary differential equation (Eq. (18)) let

$$Y(\eta)=\sum_{n=0}^{\infty}c_n\eta^n, \quad (26)$$

using a different independent variable $\eta=\bar{y}$. Moreover, Eqs. (22b) and (22c) provide the first and second derivatives for $Y(\eta)$ in Eq. (26). Following substitution in the differential equation (Eq. (18)) and, after removing the zero terms, one obtains

$$\sum_{n=2}^{\infty}c_n n(n-1)\eta^{n-2}+\omega^2\psi[1-\beta\cosh(\omega\eta)]\sum_{n=0}^{\infty}c_n\eta^n=0. \quad (27)$$

After substituting for

$$\beta\cosh(\omega\eta)=\sum_{i=0}^{\infty}a_i\eta^i, \quad (28a)$$

where

$$a_i=\begin{cases}\frac{\beta}{i!}(\omega)^i & \text{when } i \text{ is even},\\ 0 & \text{when } i \text{ is even}.\end{cases} \quad (28b)$$

In Eq. (27), it can be written as

$$\sum_{n=2}^{\infty}c_n n(n-1)\eta^{n-2}+\omega^2\psi\sum_{n=0}^{\infty}c_n\eta^n-\omega^2\psi\sum_{n=0}^{\infty}d_n\eta^n=0, \quad (29a)$$

where

$$d_n=\sum_{j=0}^{n}c_j a_{n-j}. \quad (29b)$$

The term that includes η^0 suggests $c_0=\text{constant}=1$ whereas the terms that include η^1 require $c_1=0$ because of symmetry at $y=0$. Accordingly, all the terms with

odd power vanish in this solution. The values of other constants are obtainable from the recursive relation

$$c_{n+2} = -\frac{\omega^2\psi(c_n - d_n)}{(n+2)^2 - (n+2)}. \tag{30}$$

Since the terms with odd power vanish, the working relations are rearranged as

$$Y(\eta) = \sum_{n=0}^{\infty} c_n \eta^{2n}, \tag{31a}$$

$$c_0 = 1 \quad \text{and} \quad c_n = -\frac{\omega^2\psi(c_{n-1} - d_{n-1})}{4n^2 - 2n} \quad \text{for } n \geqslant 1. \tag{31b}$$

Also, Eq. (29a) is rearranged to take the form

$$\beta\cosh(\omega\eta) = \sum_{i=0}^{\infty} \frac{\beta}{(2i)!}(\omega\eta)^{2i}. \tag{32a}$$

This causes the parameter a_i in Eq. (28b) to take the form

$$a_i = \frac{\beta}{(2i)!}(\omega)^{2i}, \tag{32b}$$

while the constant d_n remains as given by Eq. (29b).

Once the solution for $Y(\bar{y})$ is known, the next step is the computation of the eigenvalues. The condition $Y(\bar{y}) = 0$ at $\bar{y} = \eta = 1$ leads toward accomplishing the task of finding the eigenvalues. Once the eigenvalues are known, the function $Y_m(\bar{y})$ describes the function $Y(\bar{y})$ for the mth eigenvalue; that is, when $\lambda = \lambda_m$ in Eq. (15). Table 1(a) contains the sample values of λ_m^2 for selected $M\,Da$ coefficients. For each case listed in Table 1(a), the first eigenvalue yields the heat transfer coefficient for thermally fully developed flow using the Eq. (4a) to get $hH/K = \lambda_1^2 D_h/(4H)$.

Table 1
Parameters for different $M\,Da$ in the temperature solution for parallel plate channels

n	$M\,Da$						
	10^{-4}	10^{-3}	10^{-2}	10^{-1}	1/4	1	10
(a) Eigenvalues λ_m^2							
1	2.44275	2.39011	2.24068	2.00029	1.94033	1.90051	1.88676
2	21.9865	21.5594	20.9343	21.0871	21.2452	21.3758	21.4256
3	61.0828	60.1016	59.5945	60.9782	61.6034	62.1034	62.2940
4	119.748	118.255	118.415	121.679	123.017	124.082	124.488
5	198.006	196.175	197.397	203.191	205.487	207.312	208.008
6	295.881	293.934	296.542	305.513	309.012	311.792	312.582
7	413.400	411.562	415.852	428.646	433.594	437.522	439.022
8	550.590	549.066	555.325	572.590	579.232	584.503	586.515
9	707.473	706.449	714.968	737.346	745.925	752.734	755.334
10	884.071	883.711	894.785	922.912	933.675	942.216	945.477
(b) Norms N_m							
1	0.505043	0.516090	0.548614	0.602659	0.617208	0.627313	0.630898
2	0.504984	0.514471	0.529844	0.567715	0.581141	0.590279	0.593428
3	0.504872	0.512277	0.524507	0.564687	0.578065	0.587193	0.590351
4	0.504715	0.510399	0.522986	0.563852	0.577223	0.586355	0.589519
5	0.504527	0.509087	0.522371	0.563510	0.576879	0.586015	0.589183
6	0.504318	0.508243	0.522063	0.563337	0.576706	0.585844	0.589014
7	0.504101	0.507706	0.521886	0.563238	0.576607	0.585747	0.588920
8	0.503886	0.507358	0.521774	0.563176	0.576545	0.585686	0.588859
9	0.503680	0.507124	0.521700	0.563134	0.576504	0.585646	0.588819
10	0.503487	0.506960	0.521644	0.563105	0.576475	0.585617	0.588791
(c) Coefficients A_m							
1	0.642889	0.655704	0.688497	0.734980	0.746777	0.754898	0.757768
2	−0.213871	−0.214446	−0.203797	−0.186169	−0.181981	−0.178908	−0.177773
3	0.127826	0.124759	0.111682	0.100174	0.976342	0.095774	0.095084
4	−0.090797	−0.086097	−0.074995	−0.066943	−0.065192	−0.063908	−0.063432
5	0.070118	0.064787	0.055719	0.049636	0.048321	0.047356	0.046998
6	−0.056897	−0.051452	−0.043968	−0.039127	−0.038083	−0.037317	−0.037033
7	0.047703	0.042405	0.036110	0.032113	0.031253	0.030622	0.030389
8	−0.040938	−0.035906	−0.03.0511	−0.027123	−0.026395	−0.025860	−0.025566
9	0.035754	0.031034	0.02.6333	0.023403	0.022774	0.022312	0.022139
10	−0.031655	−0.02725	−0.02.3110	−0.020531	−0.019978	−0.019572	−0.019421

Following the computation of the eigenvalues, the thermal condition at the entrance location provides the constants B_m in Eq. (14). The use of a constant temperature at $\bar{x} = 0$; that is, $\theta(0, \bar{y}) = 1$, greatly simplifies the determination of B_m. As an intermediate step, it is necessary to utilize the orthogonality condition

$$\int_0^1 \left(\frac{u}{U}\right) Y_m(\bar{y}) Y_n(\bar{y})\, \mathrm{d}\bar{y} = \begin{cases} 0 & \text{when } n \neq m, \\ N_m & \text{when } n \neq m, \end{cases} \tag{33a}$$

and a Graetz-solution type of analysis provides the norm

$$N_m = \int_0^1 \left(\frac{u}{U}\right) [Y_m(\bar{y})]^2\, \mathrm{d}\bar{y} = \frac{1}{2\lambda_m} \left[\frac{\partial Y_m(\bar{y})}{\partial \bar{y}}\right]_{\bar{y}=1} \left[\frac{\partial Y_m(\bar{y})}{\partial \lambda_m}\right]_{\bar{y}=1}. \tag{33b}$$

Also, the utilization of the orthogonality condition leads toward the determination of the integral that reduces to

$$A_m = \int_0^1 \left(\frac{u}{U}\right) Y_m(\bar{y})\, \mathrm{d}\bar{y} = -\frac{1}{\lambda_m^2} \left[\frac{\partial Y_m(\bar{y})}{\partial \bar{y}}\right]_{\bar{y}=1} \tag{33c}$$

when integrating Eq. (13b) over $\bar{y}$. These forms of Eqs. (33b) and (33c) remain the same for any u/U function. Finally, the use of the initial condition and orthogonality condition yield the coefficient B_m as

$$B_m = \frac{A_m}{N_m} = -\left(\frac{2}{\lambda_m}\right) \Bigg/ \left[\frac{\partial Y_m(\bar{y})}{\partial \lambda_m}\right]_{\bar{y}=1}. \tag{34}$$

Table 1(b) is prepared to show a sample value of the computed norm N_m for the same MDa values appearing in Table 1(a). Moreover, Table 1(c) is prepared to demonstrate corresponding computed values of coefficient A_m. All entries listed in these tables have accurate figures. Finally, the temperature solution is obtainable after substituting for B_m from Eq. (34) in Eq. (14).

To avoid redundancy, a presentation of the temperature solution will appear later. The main objective of this study is the computation of local and average heat transfer coefficients. For parallel plate channels, L_c is selected as H and then Eq. (4a) provides the local dimensionless heat transfer coefficient. Fig. 2(a) shows the computed local dimensionless heat transfer coefficient hH/k plotted versus $\bar{x} = x/(PeH)$ using 35–50 eigenvalues depending on the value of MDa. The data in a log–log plot show near linear behavior as $\bar{x}$ goes toward zero. A mixed symbolic and numerical computation was used to accomplish this task. The computation of eigenvalues when m is large becomes demanding. Using Mathematica [16], a mixed symbolic and numerical procedure with a high degree of precision was written to perform the task of finding these eigenvalues. Next, the dimensionless average heat transfer coefficient $\bar{h}H/k$ (see Eq. (5b)) is plotted versus $\bar{x}$ in Fig. 2(b). Because a relatively small number of eigenvalues was used, a second method of solution is employed in order to verify the accuracy of the results; this comparison is discussed in a separate section.

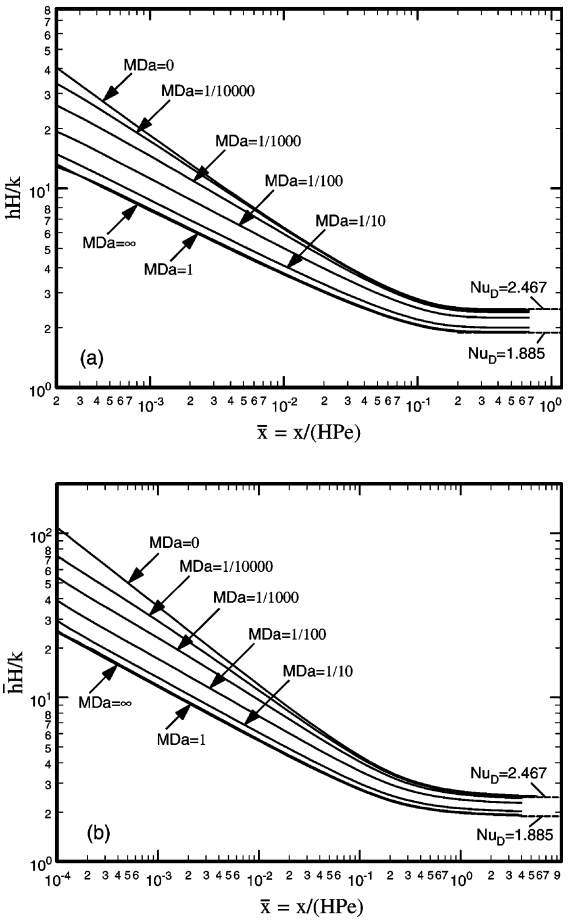

Fig. 2. Heat transfer coefficient in a parallel plate channel for different MDa coefficients: (a) local and (b) average.

4. Velocity and temperature fields in circular pipes

Consideration is given to heat transfer to a fluid passing through a porous medium bounded by an impermeable circular wall (see Fig. 3). The procedure to obtain a temperature solution is similar to that described for the parallel plate channel. The second method used earlier is modified here. In cylindrical coordinates, the momentum equation is

$$\mu_e \left(\frac{\partial^2 u}{\partial r^2} + \frac{1}{r}\frac{\partial u}{\partial r}\right) - \frac{\mu}{K} u - \frac{\partial p}{\partial x} = 0, \tag{35}$$

where r is the local radial coordinate and x is the axial coordinate (Fig. 3). If the pipe radius is designated by r_o

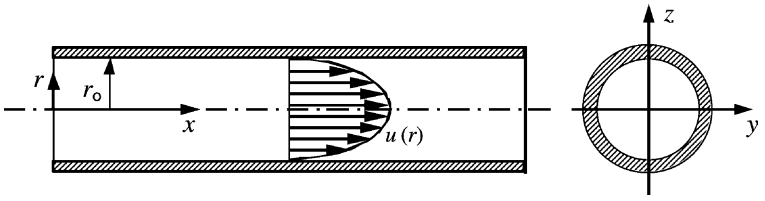

Fig. 3. Schematic of a flow in a circular pipe.

and $L_c = r_o$, the dimensionless quantities defined for flow in parallel plate channels are repeated after some modifications; the modified quantities are: $L_c = r_o$, $\bar{r} = r/r_o$, $\bar{u} = \mu u/(\Phi r_o^2)$, $Da = K/r_o^2$, and $\omega = (MDa)^{-1/2}$. Then, the momentum equation reduces to

$$M\left(\frac{d^2\bar{u}}{d\bar{r}^2} + \frac{1}{\bar{r}}\frac{d\bar{u}}{d\bar{r}}\right) - \frac{u}{Da} + 1 = 0. \tag{36}$$

Using the boundary condition $\bar{u} = 0$ at $\bar{r} = 1$ and the condition $\partial\bar{u}/\partial\bar{r} = 0$ at $\bar{r} = 0$, the solution becomes

$$\bar{u} = Da\left[1 - \frac{I_0(\omega\bar{y})}{I_0(\omega)}\right], \tag{37}$$

where, as before, $\omega = (MDa)^{-1/2}$. Here, the mean velocity defined by the relation

$$U = \frac{2}{r_o^2}\int_0^{r_o} ur\,dr, \tag{38}$$

and the velocity profile take the form

$$\frac{u}{U} = \frac{\bar{u}}{\overline{U}} = \frac{\omega I_0(\omega)}{\omega I_0(\omega) - 2I_1(\omega)}\left[1 - \frac{I_0(\omega\bar{r})}{I_0(\omega)}\right]. \tag{39}$$

Using the computed values of $\overline{U} = Da[1 - (2/\omega)I_1(\omega)/I_0(\omega)]$, the relation

$$f = -\frac{(\partial p/\partial x)D_h}{\rho U^2/2} = \frac{2}{\overline{U}}\frac{1}{Re_D}\left(\frac{D_h}{r_o}\right)^2 \tag{40}$$

provides the pipe pressure drop.

The steady-state form of the energy equation in cylindrical coordinates is

$$u\frac{\partial T}{\partial x} = \frac{k}{\rho c_p}\left(\frac{\partial^2 T}{\partial r^2} + \frac{1}{r}\frac{\partial T}{\partial r}\right). \tag{41}$$

Defining the dimensionless temperature $\theta = (T - T_w)/(T_i - T_w)$ where T_i is the inlet temperature and T_w is the wall temperature, one obtains

$$\frac{u}{U}\frac{\partial\theta}{\partial\bar{x}} = \frac{\partial^2\theta}{\partial\bar{r}^2} + \frac{1}{\bar{r}}\frac{\partial\theta}{\partial\bar{r}}, \tag{42}$$

where $\bar{x} = x/(Pe\,r_o)$ and $Pe = \rho c_p r_o U/k$. As before, separating the variables, $\theta(\bar{x},\bar{r}) = X(\bar{x})R(\bar{r})$ leads to solution of two ordinary differential equations,

$$X'(\bar{x}) + \lambda^2 X(\bar{x}) = 0 \tag{43a}$$

and

$$R''(\bar{r}) + \frac{1}{\bar{r}}R'(\bar{r}) + \lambda^2\left(\frac{u}{U}\right)R(\bar{r}) = 0. \tag{43b}$$

The major task remaining is to find the exact value of $R(\bar{r})$ and its verification by comparing it with the numerically obtained data. The parameter λ in Eq. (43b) serves as the eigenvalue. The final temperature solution, after the computation of eigenvalues, is

$$\theta = \sum_{m=1}^{\infty} B_m R_m(\bar{r})e^{-\lambda_m^2\bar{x}}. \tag{44}$$

Eq. (43b) following substitution for u/U takes the following form:

$$R''(\bar{r}) + \frac{1}{\bar{r}}R'(\bar{r}) + \lambda^2\left\{\frac{\omega I_0(\omega)}{\omega I_0(\omega) - 2I_1(\omega)} \times \left[1 - \frac{I_0(\omega\bar{r})}{I_0(\omega)}\right]\right\}R(\bar{r}) = 0. \tag{45}$$

Using the abbreviations

$$\beta = 1/I_0(\omega) \tag{46a}$$

and

$$\psi = \frac{I_0(\omega)}{\omega I_0(\omega) - 2I_1(\omega)}\frac{\lambda^2}{\omega}, \tag{46b}$$

in the following analysis, Eq. (45) is rewritten as

$$R''(\bar{r}) + \frac{1}{\bar{r}}R'(\bar{r}) + \omega^2\psi\left[1 - \beta I_0(\omega\bar{r})\right]R(\bar{r}) = 0. \tag{46c}$$

Eq. (46c) is subject to the boundary conditions $R'(0) = R(1) = 0$. Similar to the previous case, one can select $\eta = I_0(\omega r) - 1$; however, this selection did not produce sufficient simplification to warrant its implementation. Therefore, a direct derivation of a series solution will follow.

Solution: To obtain this solution, let $\eta = \bar{r}$ and then set

$$R(\eta) = \sum_{n=0}^{\infty} c_n\eta^n \tag{47}$$

then

$$\frac{dR(\eta)}{d\eta} = \sum_{n=0}^{\infty} c_n n \eta^{n-1} \quad \text{for } n > 0 \tag{48a}$$

and

$$\frac{d^2R(\eta)}{d\eta^2} = \sum_{n=0}^{\infty} c_n n(n-1)\eta^{n-2} \quad \text{for } n > 1. \tag{48b}$$

After removing the zero terms in Eqs. (48a) and (48b), the substitution $R(\eta)$ and its derivatives in Eq. (46c) yields

$$\sum_{n=2}^{\infty} c_n n(n-1)\eta^n + \sum_{n=1}^{\infty} c_n n \eta^n + (\omega\eta)^2 \psi \times [1 - \beta I_0(\omega\eta)] \sum_{n=0}^{\infty} c_n \eta^n = 0. \tag{49}$$

After substituting for

$$\beta I_0(\omega\eta) = \sum_{i=0}^{\infty} a_i \eta^i, \tag{50}$$

Eq. (49) can be written as

$$\sum_{n=2}^{\infty} c_n n(n-1)\eta^n + \sum_{n=1}^{\infty} c_n n \eta^n + \omega^2 \psi \sum_{n=0}^{\infty} c_n \eta^{n+2} - \omega^2 \psi \sum_{n=0}^{\infty} d_n \eta^{n+2} = 0, \tag{51a}$$

where

$$d_n = \sum_{j=0}^{n} c_j a_{n-j}. \tag{51b}$$

The term that includes η^0 suggests $c_0 = \text{constant} = 1$ whereas the terms that include η^1 require $c_1 = 0$.

Table 2
Parameter for different $M\,Da$ in the temperature solution for circular pipes

n	$M\,Da$						
	10^{-4}	10^{-3}	10^{-2}	10^{-1}	1/4	1	10
(a) Eigenvalues λ_m^2							
1	5.66823	5.42732	4.78988	3.96224	3.79632	3.69438	3.66064
2	29.8685	28.6766	26.2350	23.4011	22.8066	22.4400	22.3186
3	73.4184	70.7493	65.8977	59.5023	58.1222	57.2731	56.9925
4	136.346	131.874	123.858	112.269	109.743	108.191	107.679
5	218.676	212.181	200.120	181.701	177.669	175.192	174.375
6	320.434	311.724	294.682	267.798	261.898	258.275	257.081
7	441.649	430.523	407.545	370.559	362.430	357.440	355.796
8	582.344	568.584	538.711	489.984	479.260	472.688	470.520
9	742.543	725.907	688.177	626.074	612.405	604.017	601.253
10	922.266	902.508	855.946	778.829	761.847	751.427	747.994
(b) Norms N_m							
1	0.137487	0.143488	0.159961	0.179869	0.18408	0.1868201	0.187759
2	0.0590511	0.0613218	0.0655328	0.0720243	0.0736315	0.0746558	0.0750002
3	0.0375695	0.0387828	0.0409746	0.0450105	0.0460102	0.0466463	0.0468598
4	0.0275390	0.0282878	0.0298015	0.0327336	0.0334597	0.0339215	0.0340765
5	0.0217298	0.0222421	0.0234160	0.0257188	0.0262891	0.0266516	0.0267733
6	0.0179401	0.0183201	0.0192840	0.0211800	0.0216495	0.0219480	0.0220482
7	0.0152729	0.0155728	0.0163915	0.0180029	0.0184019	0.0186557	0.0187450
8	0.0132940	0.0135417	0.0142535	0.0156547	0.0160019	0.0162181	0.0163021
9	0.0117676	0.0119793	0.0126089	0.0138483	0.0141553	0.0143504	0.0144238
10	0.0105547	0.0107401	0.0113046	0.0124158	0.0126909	0.0128659	0.0129250
(c) Coefficients A_m							
1	0.220128	0.228737	0.248854	0.269514	0.273661	0.276348	0.277268
2	−0.062696	−0.063753	−0.062333	−0.060905	−0.060710	−0.060557	−0.060498
3	0.031764	0.031356	0.029049	0.027938	0.027775	0.027654	0.027609
4	−0.019841	−0.019012	−0.017190	−0.016449	−0.016338	−0.016257	−0.016227
5	0.013818	0.012901	0.0115313	0.011009	0.010931	0.010873	0.010852
6	−0.010287	−0.0094039	−0.0083552	−0.0079669	−0.007908	−0.0078656	−0.0078497
7	0.0080122	0.0072030	0.0063781	0.0060771	0.0060316	0.0059984	0.0059881
8	−0.0064475	−0.0057215	−0.0050555	−0.0048145	−0.0047783	−0.0047514	−0.0047389
9	0.0053188	0.0046725	0.0041228	0.0039249	0.0038949	0.0038730	0.0038683
10	−0.0044743	−0.0039015	−0.0034376	−0.0032718	−0.0032466	−0.0032282	−0.0032212

Accordingly, all the terms with odd power vanish in the solution. The values of other constants are obtainable from the recursive relation

$$c_{n+2} = -\frac{\omega^2\psi(c_n + d_n)}{(n+2)^2}. \tag{52}$$

Since the terms with odd power vanish, the working equation may be rewritten as

$$R(\eta) = \sum_{n=0}^{\infty} c_n \eta^{2n}, \tag{53a}$$

$$c_0 = 1, \quad c_n = -\frac{\omega^2\psi(c_{n-1} - d_{n-1})}{4n^2} \quad \text{for } n \geqslant 1. \tag{53b}$$

Moreover, the relation

$$\beta I_0(\omega\eta) = \sum_{i=0}^{\infty} \frac{\beta}{(i!)^2}\left(\frac{\omega\eta}{2}\right)^{2i} \tag{54a}$$

makes

$$a_i = \frac{\beta}{(i!)^2}\left(\frac{\omega}{2}\right)^{2i}, \tag{54b}$$

and the constant d_n remains as

$$d_{2n} = \sum_{j=0}^{n} c_j a_{n-j} \tag{54c}$$

for insertion in this recursive relation.

As for the previous case, the solution for $R(\bar{r})$ must satisfy the condition $R(\bar{r}) = 0$ when $\bar{r} = \eta = 1$. This condition leads toward the computation of eigenvalues. The first 10 eigenvalues for selected MDa values are listed in Table 2(a). Accordingly, the function $R_m(\bar{r})$, in Eq. (44), describes the function $R(\bar{r})$ for the mth eigenvalue; that is, when $\lambda = \lambda_m$ also in Eq. (44). To compute B_m for inclusion in Eq. (44), one needs to use the thermal condition at the entrance location; that is $\theta(0, \bar{y}) = 1$ at $\bar{x} = 0$ in this study. The analysis leads to the following orthogonality condition

$$\int_0^1 \left(\frac{u}{U}\right)\bar{r}R_m(\bar{r})R_n(\bar{r})\,\mathrm{d}\bar{r} = \begin{cases} 0 & \text{when } n \neq m, \\ N_m & \text{when } n \neq m, \end{cases} \tag{55a}$$

where the norm N_m assumes the following form:

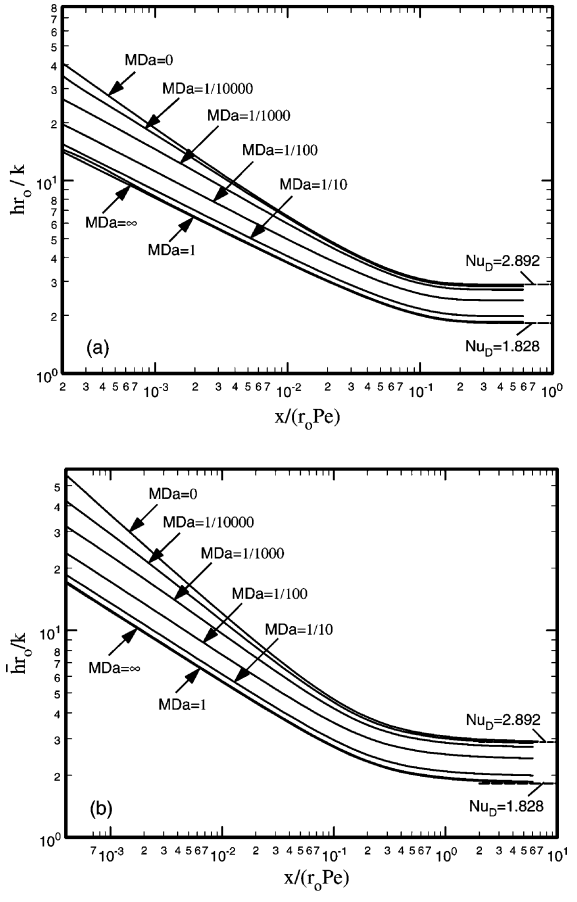

Fig. 4. Heat transfer coefficient in circular pipes for different MDa coefficients: (a) local and (b) average.

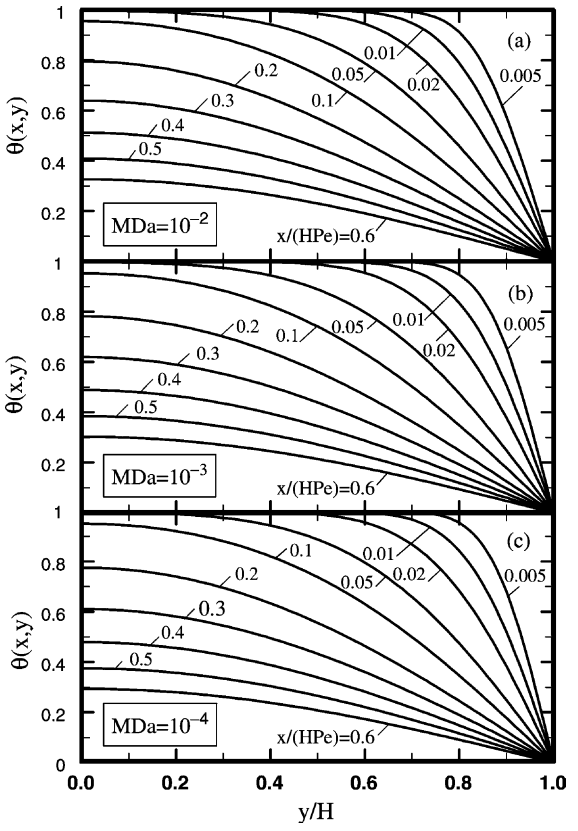

Fig. 5. Temperature distribution in the thermal entrance region of parallel plate channels when (a) $MDa = 10^{-2}$, (b) $MDa = 10^{-3}$, and (c) $MDa = 10^{-4}$.

$$N_m = \int_0^1 \left(\frac{u}{U}\right)\bar{r}[R_m(\bar{r})]^2\,\mathrm{d}\bar{r} = \frac{1}{2\lambda_m}\left[\frac{\partial R_m(\bar{r})}{\partial \bar{r}}\right]_{\bar{r}=1}\left[\frac{\partial R_m(\bar{r})}{\partial \lambda_m}\right]_{\bar{r}=1}, \tag{55b}$$

and the determination of coefficient A_m followed by integrating Eq. (43b) after replacing λ with λ_m and R with R_m yields

$$A_m = \int_0^1 \left(\frac{u}{U}\right)\bar{r}R_m(\bar{r})\,\mathrm{d}\bar{r} = -\frac{1}{\lambda_m^2}\left[\frac{\partial R_m(\bar{r})}{\partial \bar{r}}\right]_{\bar{r}=1}. \tag{55c}$$

Finally, the coefficients B_m for inclusion in Eq. (44) is

$$B_m = \frac{A_m}{N_m} = -\left(\frac{2}{\lambda_m}\right)\Big/\left[\frac{\partial R_m(\bar{r})}{\partial \lambda_m}\right]_{\bar{r}=1}. \tag{56}$$

Table 2(b) is prepared to show the computed norms N_m corresponding to the eigenvalues listed in Table 2(a). To facilitate the computation of B_m from Eq. (56) for inclusion in Eq. (44), Table 2(c) contains the coefficients A_m computed using Eq. (55c).

For circular pipes, r_o replaces L_c in Eqs. (4a) and (5b) and they can be used to compute fluid temperature (Eq. (44)); a temperature solution presentation will appear later. Subsequently, the computed bulk temperature leads toward the determination of heat transfer coefficients. Fig. 4(a) shows the computed dimensionless local heat transfer coefficient hr_o/k plotted versus $\bar{x}$ using 50 eigenvalues in a Graetz-type solution. As in the previous case, the data, in a log–log plot, show near linear behavior as $\bar{x}$ goes toward zero. Fig. 4(b) shows the dimensionless average heat transfer coefficient $\bar{h}r_o/k$ plotted versus $\bar{x}$. These data are also to be compared with data obtained using an alternative method of solution.

The temperature solution, using the aforementioned exact analysis provided accurate results when x is relatively large. However, it became a cumbersome task to evaluate all needed eigenvalues for any arbitrarily selected MDa at extremely small values of $\bar{x}$. Because the computer capacity limits the needed number of eigenvalues, an alternative method of analysis is the subject of the following studies.

5. An alternative method of solution

As stated earlier, it is difficult to obtain many eigenvalues using the exact analysis. This is due to round-off errors caused by the finiteness of machine capacity and computational speed. Therefore, for a finite number of eigenvalues, it is best to optimize the solution using variational calculus. This type of analysis leads to a Green's function solution method that uses the weighted residuals technique. The temperature solution is similar to that for transient heat conduction in Beck et al. [11, Chapter 10] when the axial coordinate x replaces time t.

The method of solution presented here equally applies to ducts described earlier and it can be extended to accommodate the ducts having various cross section shapes. As significant advantages, the computation of eigenvalues is automatic, and the computation of other coefficients is also automatic. In this technique, for preselected M eigenvalues, the proposed solution is a modification of Eq. (14), that is,

$$\theta = \sum_{m=1}^{\infty} B_m \Psi_m(\bar{y})\mathrm{e}^{-\lambda_m^2\bar{x}}, \tag{57a}$$

where

$$\Psi_m(\eta) = \sum_{j=1}^{N} d_{mj} f_j(\eta), \tag{57b}$$

and the function $f_j(\eta)$ are selected so that they satisfy the homogeneous boundary conditions along the surface of the ducts; that is,

$$f_j(\eta) = (1-\eta^2)\eta^{2(j-1)}. \tag{57c}$$

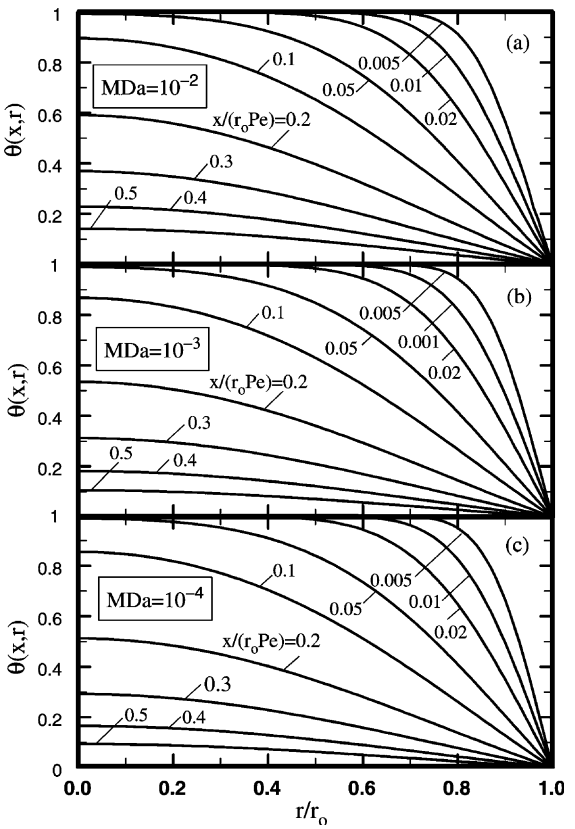

Fig. 6. Temperature distribution in the thermal entrance region of circular pipes when (a) $MDa = 10^{-2}$, (b) $MDa = 10^{-3}$, and (c) $MDa = 10^{-4}$.

For a parallel plate channel $\Psi_m(\eta)$ stands for $Y_m(\eta)$ and for a circular pipe $\Psi_m(\eta)$ stands for $R_m(\eta)$. The remaining steps apply equally to both cases with minor modifications to be identified later.

As described in Beck et al. [11], the next task is the computation of eigenvalues λ_m^2 and the coefficients d_{mj} in Eq. (57b). The computation begins by finding the elements of two matrices, **A** and **B**,

$$a_{ij} = \int_0^1 f_i(\eta)\nabla^2 f_j(\eta) J \,\mathrm{d}\eta \tag{58a}$$

and

$$b_{ij} = \int_0^1 \rho c_\mathrm{p}\left(\frac{u}{U}\right) f_i(\eta) f_j(\eta) J \,\mathrm{d}\eta. \tag{58b}$$

The parameter J in Eqs. (58a) and (58b) is the Jacobian; $J = 1$ for parallel plate channels and $J = \eta$ is for circular ducts. This analysis leads to an eigenvalue problem [11]

$$(\mathbf{A} + \lambda^2 \mathbf{B})\mathbf{d} = 0, \tag{59a}$$

that can be rewritten as

$$(\mathbf{B}^{-1}\mathbf{A} + \lambda^2 \mathbf{I})\mathbf{d} = 0. \tag{59b}$$

The symbolic software Mathematica was used to produce the elements of matrices **A** and **B** and subsequently the eigenvalues λ_m^2 and the corresponding coefficients d_{mj} embedded within the eigenvectors **d**. The basic Mathematica statements to accomplish this task, when using Eqs. (58a) and (58b) for a parallel plate channel, are

```
fi = (1-x^2) * x^(2*i-2);
fj = (1-x^2) * x^(2*j-2);
oper = Simplify[fi*(D[D[fj,x],x])];
amat = Table[Integrate[oper, {x,0,1}], {i,1,m},
{j,1,m}];
bmat = Table[Integrate[cap*u*fi*fj/uav, {x,0,1}],
{i,1,m}, {j,1,m}];
eigv = N[Eigenvalues[-Inverse[bmat].amat]];
dvect = Eigenvectors[-Inverse[bmat].amat];
```

In the computer code above, x stands for η, amat = **A**, bmat = **B**, uav = U, cap = ρc_p, while eigv is a vector containing the eigenvalues and dvect contains the eigenvectors within its rows. The remaining parameters are the same as those presented earlier in the text and in the nomenclature. The eigenvectors in Mathematica appear as the rows of a matrix to be designated as **D**.

Table 3
Comparison of computed data for parallel plate channels

MDa	$\frac{(x/D_\mathrm{h})}{Re_D Pr}$	$[Nu_D]_{\mathrm{Ex}}$ [a]	$[Nu_D]_{\mathrm{WR}}$ [b]	$[\overline{Nu}_D]_{\mathrm{Ex}}$ [a]	$[\overline{Nu}_D]_{\mathrm{WR}}$ [b]	$[\theta_\mathrm{b}]_{\mathrm{Exact}}$
10^{-2}	10^{-4}	38.074	38.074	58.383	58.383	0.97692
	5×10^{-4}	21.634	21.634	33.275	33.275	0.93562
	10^{-3}	17.053	17.053	26.127	26.127	0.90077
	5×10^{-3}	10.516	10.516	15.249	15.249	0.73714
	10^{-2}	9.3025	9.3025	12.502	12.502	0.60648
	5×10^{-2}	8.9626	8.9626	9.6932	9.6932	0.14390
	10^{-1}	8.9626	8.9626	9.3279	9.3279	0.2397×10^{-1}
	0.5	8.9626	8.9626	9.0356	9.0356	0.1418×10^{-7}
10^{-3}	10^{-4}	48.638	48.637	77.477	77.479	0.96948
	5×10^{-4}	25.806	25.806	42.049	42.048	0.91934
	10^{-3}	19.672	19.672	32.143	32.143	0.87935
	5×10^{-3}	11.377	11.377	17.529	17.529	0.70427
	10^{-2}	9.9424	9.9424	14.001	14.001	0.57118
	5×10^{-2}	9.5605	9.5605	10.474	10.474	0.12311
	10^{-1}	9.5605	9.5605	10.017	10.017	0.1819×10^{-1}
	0.5	9.5605	9.5605	9.6518	9.6518	0.4136×10^{-8}
10^{-4}	10^{-4}	56.280	56.271	96.297	96.319	0.96221
	5×10^{-4}	27.624	27.623	48.570	48.572	0.90743
	10^{-3}	20.587	20.587	36.036	36.037	0.86576
	5×10^{-3}	11.625	11.625	18.630	18.630	0.68894
	10^{-2}	10.149	10.149	14.661	14.661	0.55630
	5×10^{-2}	9.7710	9.7710	10.773	10.773	0.11594
	10^{-1}	9.7710	9.7710	10.272	10.272	0.1643×10^{-1}
	0.5	9.7710	9.7710	9.8712	9.8712	0.2667×10^{-8}

[a] Nusselt number from exact analysis.
[b] Nusselt number using method of weighted residuals.

One can show that the eigenfunctions $\Psi_m(\eta)$ are orthogonal; however with matrices **B** and **D** in hand, the coefficients B_m for inclusion in Eq. (14) are obtainable from the relation [11, Eq. (10.53)],

$$B_m = \sum_{i=1}^{N} p_{mi} \int_0^1 \rho c_p \left(\frac{u}{U}\right) f_i(\eta)\, d\eta. \tag{60}$$

The parameters p_{mi} in Eq. (60) are the elements of a matrix

$$\mathbf{P} = [(\mathbf{D}\cdot\mathbf{B})^{T}]^{-1}, \tag{61}$$

that is, the matrices **D** multiplied by matrix **B** and the resulting matrix is transposed and then inverted. Following computation of **D** and **P**, the Green's function is readily available to include the effect of frictional heating (see Beck et al. [11, p. 308]). This task can be performed conveniently using Mathematica [16]. This numerical computation of temperature can be extended to passages having various shapes, e.g., triangular ducts, etc. The needed modifications are described in Refs. [11,17]. It should be stated that both the exact values of velocity and a computed velocity using the classical Galerkin method [17] were used and the results show insignificant difference in the temperature data.

6. Numerical results

As a first test of these two solution methods, the temperature distribution in parallel plate channels are presented in Fig. 5. The data show the temperature field in the entrance region under the conditions (a) when $MDa = 10^{-2}$, (b) when $MDa = 10^{-3}$, and (c) when $MDa = 10^{-4}$. The data show a slight increase in the slope at the wall as MDa decrease. Fig. 6 repeats the presentation of temperature fields for flow in circular pipes and the temperature in the entrance region are for

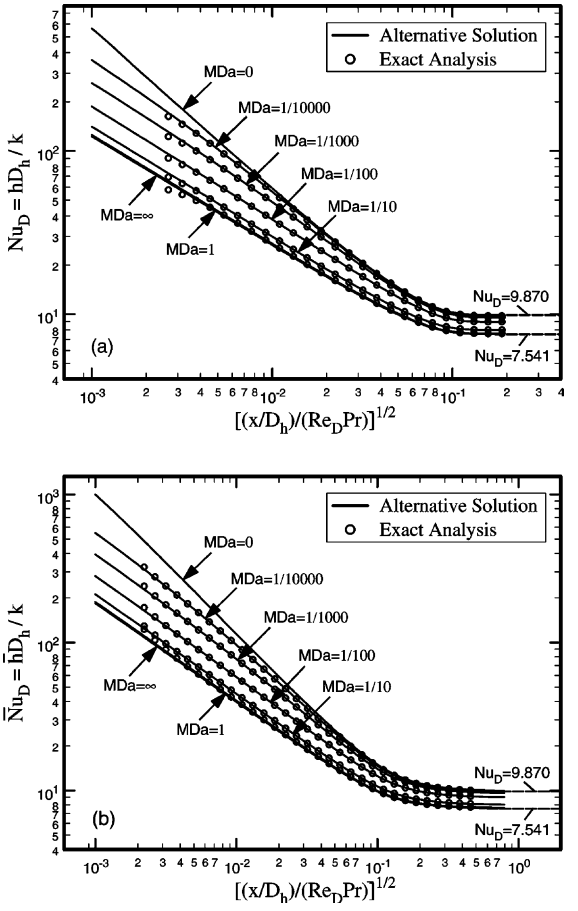

Fig. 7. Comparison of the local heat transfer coefficient obtained by two methods in a parallel plate channel for different MDa coefficients: (a) local and (b) average.

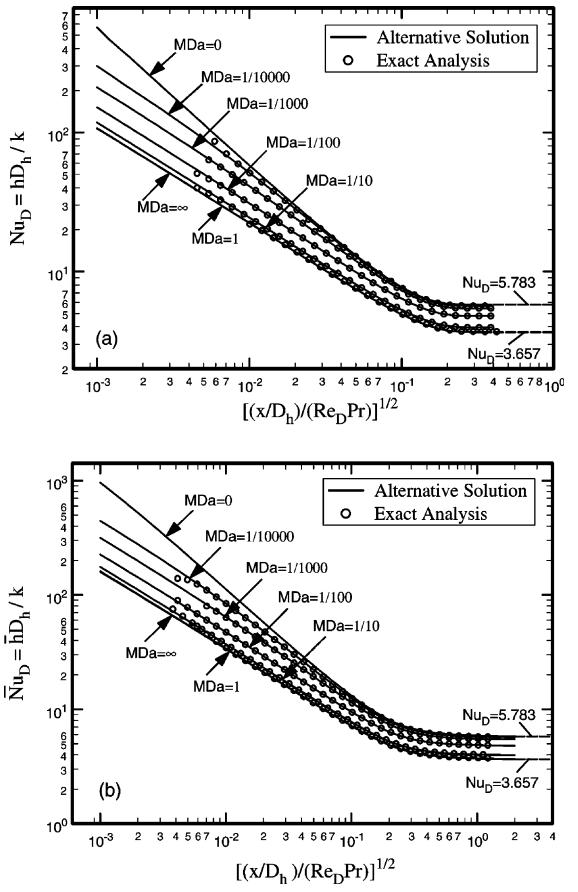

Fig. 8. Comparison of the local heat transfer coefficient obtained by two methods in a circular pipe for different MDa coefficients: (a) local and (b) average.

the conditions (a) when $MDa = 10^{-2}$, (b) when $MDa = 10^{-3}$, and (c) when $MDa = 10^{-4}$. The temperature fields plotted in Figs. 5 and 6 have noticeably different distribution patterns.

Following the computation of temperature, the next task is to compute local and average heat transfer coefficients for fluid flowing through parallel plate ducts and circular pipes within the range of $10^{-6} \leqslant (x/D_h)/(Re_D Pr) < \infty$ where $D_h = 4A/C$, $Re_D = \rho U D_h/\mu$, and $Pr = \mu c_p/k$. As many as 50 eigenvalues did not provide results with sufficient accuracy using the exact analysis; however, 40 eigenvalues did yield relatively accurate results using this alternative solution. The data in Table 3 show excellent agreement between computed local heat transfer coefficients within a small range of the dimensionless axial coordinate (see Columns 2 and 3). Also, these two completely different methods of solution yield the average heat transfer coefficients in Columns 5 and 6 that are in excellent agreement. For a larger range of the dimensionless axial coordinate, Fig. 7 is prepared to demonstrate graphically the agreement between these two solution methods. Fig. 7(a) shows the local heat transfer coefficient for flow between two parallel plates filled with porous materials. The solid lines in Fig. 7(a) are obtained using this alternative analysis using 40 eigenvalues. The graph shows the local Nusselt number $Nu_D = hD_h/k = 4hH/k$, for various MDa values, plotted versus $\sqrt{(x/D_h)/(Re_D Pr)} = \sqrt{\bar{x}/16}$. The solid lines in

Table 4
Comparison of computed data for cylindrical pipes

MDa	$\frac{(x/D_h)}{Re_D Pr}$	$[Nu_D]_{Ex}$ [a]	$[Nu_D]_{WR}$ [b]	$[\overline{Nu}_D]_{Ex}$ [a]	$[\overline{Nu}_D]_{WR}$ [b]	$[\theta_b]_{Exact}$
10^{-2}	5×10^{-4}	17.447	17.447	26.938	26.938	0.94755
	10^{-3}	13.645	13.645	21.093	21.093	0.91909
	5×10^{-3}	7.8710	7.8710	11.999	11.999	0.78665
	10^{-2}	6.3810	6.3810	9.4985	9.4985	0.68390
	5×10^{-2}	4.8349	4.8349	6.0584	6.0584	0.29770
	10^{-1}	4.7905	4.7905	5.4293	5.4293	0.11398
	0.5	4.7899	4.7899	4.9178	4.9178	0.5351×10^{-4}
	1	4.7899	4.7899	4.8538	4.8538	0.3699×10^{-8}
10^{-3}	5×10^{-4}	22.272	22.251	35.482	35.541	0.93149
	10^{-3}	17.010	17.002	27.354	27.377	0.89636
	5×10^{-3}	9.2264	9.2255	14.828	14.830	0.74338
	10^{-2}	7.3122	7.3119	11.464	11.465	0.63221
	5×10^{-2}	5.4677	5.4677	6.9970	6.9972	0.24674
	10^{-1}	5.4277	5.4277	6.2165	6.2166	0.8319×10^{-1}
	0.5	5.4273	5.4273	5.5852	5.5852	0.1409×10^{-4}
	1	5.4273	5.4273	5.5062	5.5062	0.2721×10^{-9}
10^{-4}	5×10^{-4}	25.650	25.647	43.943	43.951	0.91587
	10^{-3}	18.942	18.941	32.842	32.845	0.87690
	5×10^{-3}	9.7254	9.7253	16.628	16.628	0.71709
	10^{-2}	7.6266	7.6265	12.556	12.556	0.60518
	5×10^{-2}	5.7043	5.7043	7.4093	7.4093	0.22721
	10^{-1}	5.6685	5.6685	6.5425	6.5425	0.7302×10^{-1}
	0.5	5.6682	5.6682	5.8431	5.8431	0.8409×10^{-5}
	1	5.6682	5.6682	5.7557	5.7557	0.1003×10^{-9}

[a] Nusselt number from exact analysis.
[b] Nusselt number using method of weighted residuals.

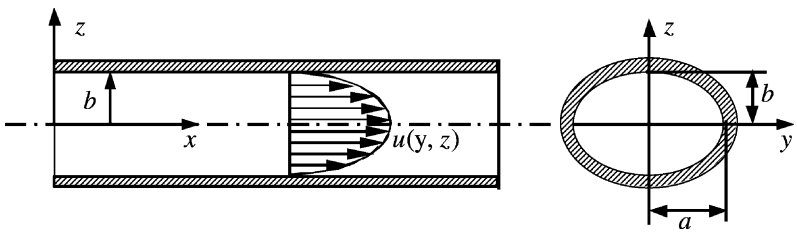

Fig. 9. Schematic of a flow in an elliptical duct.

Fig. 7(b) show the average Nusselt number, $\overline{Nu}_D = \bar{h}D_h/k = 4\bar{h}H/k$, plotted versus $\sqrt{(x/D_h)/(Re_D Pr)} = \sqrt{\bar{x}/16}$. The solid lines in Fig. 7(b) show similar characteristics to those in Fig. 7(a). At lower values of $\bar{x}$, the slope in Fig. 7(b) is nearly linear and it is similar to that in Fig. 7(a); however, the Nusselt number values are higher as expected. The discrete circular symbols, in Fig. 7(a) and (b), are from the exact analysis using 50 eigenvalues. These two sets of data agree well at larger values of x. However, the discrete data exhibit a sudden departure from a near linear form at their lowest plotted values of the dimensionless axial coordinate. This phenomenon appears when the number of eigenvalues is insufficient. As a remedy, the space partitioning similar to time partitioning [11] can be effective.

For flow in circular ducts filled with porous materials, the solid lines in Fig. 8(a) show the computed local heat transfer coefficients for various MDa values. For a circular pipe, the Nusselt number $Nu_D = hD_h/k = 2hr_o/k$ is plotted versus $\sqrt{(x/D_h)/(Re_D Pr)}$. As in the previous case, the data properly approach the limiting values: unobstructed tube flow when $MDa \to \infty$ and that for slug flow when $MDa \to 0$. The data in this figure clearly indicate that the first eigenvalue in Table 2(a) directly represents the fully developed Nusselt number for various MDa values. The average Nusselt number is plotted, using solid lines, in Fig. 8(b). They show the variation of the average Nusselt number $\overline{Nu}_D = \bar{h}D_h/k = 2\bar{h}r_o/k$ as a function of $\sqrt{(x/D_h)/(Re_D Pr)} = \sqrt{\bar{x}/4}$. The circular symbols in Fig. 8(a) and (b) represent exact analysis using 50 eigenvalues. The data in Fig. 8(b) show trends similar to the data in Fig. 8(a) except they have higher values. A numerical comparison for these two solutions is Table 4. The entries in this table show that both solution methods agree well, except at very small values of x.

7. Discussion

For comparison, the symbols in Fig. 2(a) and (b) are the data plotted in Fig. 7(a) and (b), respectively. Similarly, the discrete data in Fig. 8(a) and (b) are taken

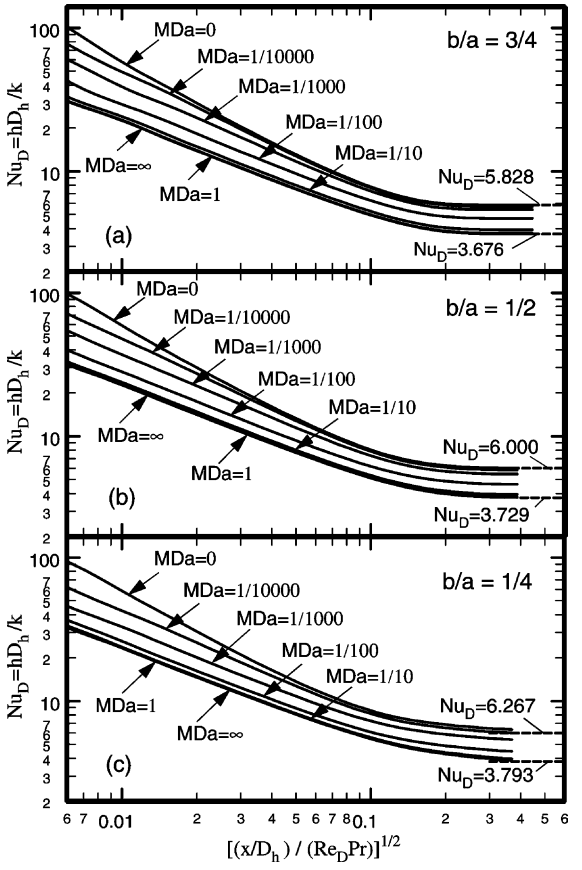

Fig. 10. Local heat transfer coefficient in elliptical ducts for different MDa values: (a) when $b/a = 0.75$, (b) when $b/a = 0.50$, and (c) when $b/a = 0.25$.

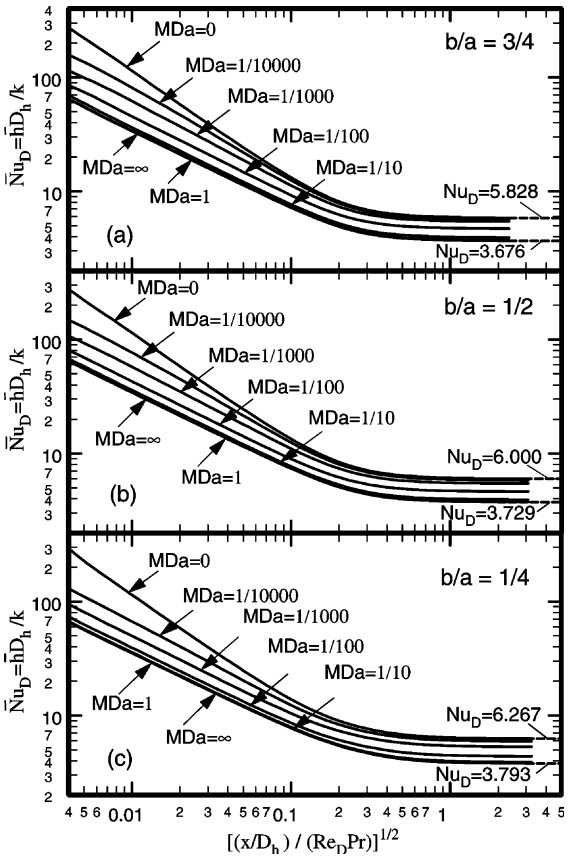

Fig. 11. Average heat transfer coefficient in elliptical ducts for different MDa values: (a) when $b/a = 0.75$, (b) when $b/a = 0.50$, and (c) when $b/a = 0.25$.

from Fig. 4(a) and (b) also to verify their accuracy. Certainly, the agreement between data obtained using these two solution methods is satisfactory. The numerical evaluation of the coefficients in the exact analysis often requires large computer word length depending on the number of eigenvalues sought. The same state of affairs was encountered using this alternative solution based on the method of weighted residuals. However, in this alternative solution, the computer computes all eigenvalues and needed coefficients directly and automatically. This is significant when the process needs to be repeated for various MDa values.

Analogous to the classical diffusion equation, one can use space partitioning in order to reduce the required number of eigenvalues once a solution at and near $x = 0$ is available. Such a study is beyond the scope of this paper. In the absence of a solution at small x, the near linear behavior of data is significant. Because, as an approximation, this line can be extended toward $x = 0$ in order to estimate the heat transfer coefficient at x values much smaller than those reported here.

As stated earlier, this alternative solution based on the method of weighted residuals, can be used to solve for temperature field and heat transfer coefficients in ducts having other shape, e.g., triangular passages. To demonstrate this, consideration is given to a fluid flow in an elliptical duct filled with porous materials. The walls of the duct are impermeable and satisfy equation $y^2/a^2 + z^2/b^2 = 1$; the coordinates and parameters a and b are depicted in Fig. 9. Assuming the wall to have a uniform temperature, the temperature solution is computed after inserting B_m from Eq. (60) in Eq. (57a). For this application, the needed modifications are the selection of a new set of basis functions and modified integrations to compute elements of matrices **A**, **B**, and coefficients B_m. For a suitable and complete set of basis functions, equation

$$f_j(y,z) = (1 - y^2/a^2 - z^2/b^2)y^{2(m_j-1)}z^{2(n_j-1)} \tag{62}$$

with appropriate values for $m_j = 1, 2, \ldots$ and $n_j = 1, 2, \ldots$ is used.

The computations are performed for three different aspect ratios: $b/a = 0.75$, 0.50, and 0.25; the computed local heat transfer coefficients are in Fig. 10(a)–(c), respectively. In these figures, the values of $Nu_D =$

Table 5
Pressure coefficient and the Nusselt number under fully developed condition for flow in elliptic passages

b/a (D_h/a)	MDa	$M\overline{U}$	λ_1^2	F/M	Nu_D ($x \to \infty$)
1/4 (0.732441)	0	0	46.72	∞	6.267
	1/10,000	0.00009457	44.22	11,350	5.931
	1/1000	0.0008316	39.62	1290	5.314
	1/100	0.005161	32.62	207.9	4.375
	1/10	0.01231	28.99	87.16	3.888
	1	0.01442	28.36	74.41	3.804
	∞	0.01471	28.28	72.96	3.793
1/2 (1.29705)	0	0	14.27	∞	6.000
	1/10,000	0.00009691	13.83	34,720	5.817
	1/1000	0.0009045	12.95	3720	5.447
	1/100	0.007131	10.99	471.8	4.622
	1/10	0.03026	9.332	111.2	3.925
	1	0.04688	8.947	71.77	3.763
	∞	0.05000	8.897	67.29	3.742
3/4 (1.70557)	0	0	8.014	∞	5.828
	1/10,000	0.00009762	7.824	59,600	5.690
	1/1000	0.0009272	7.440	6275	5.411
	1/100	0.007793	6.467	746.6	4.703
	1/10	0.04162	5.392	139.8	3.921
	1	0.08039	5.095	72.37	3.705
	∞	0.090000	5.055	64.64	3.676
1 (2)	0	0	5.783	∞	5.783
	1/10,000	0.0000980	5.668	81,624	5.668
	1/1000	0.0009378	5.438	8531	5.438
	1/100	0.008103	4.790	987.3	4.790
	1/10	0.04806	3.962	166.5	3.962
	1	0.1072	3.661	74.61	3.661
	∞	0.1250	3.657	64.00	3.657

$hD_h/k$are plotted versus $\sqrt{(x/D_h)/(Re_D Pr)}$. Moreover, the average heat transfer coefficient is computed using Eq. (5c) and plotted in Fig. 11(a)–(c) also for $b/a = 0.75$, 0.50, and 0.25. The data are well behaved and show the same trends as those for circular passages.

Table 5 is prepared to provide information concerning limits of certain parameters. It contains the value of $\overline{U} = \mu U/(\Phi H^2)$ and the first eigenvalue λ_1^2 for selected MDa coefficients and for $b/a = 1/4$, 1/2, 3/4, and 1. These $\overline{U}$ and λ_1^2 values provide the Moody-type friction factor and the Nusselt number under hydrodynamically and thermally fully developed condition. For this reason, the pressure coefficient $F = 2(D_h/L_e)^2/\overline{U}$ that yields $f = F/Re_D$ and Nu_D for fully developed condition are also available in Table 5. The data for $b/a = 1$ are included to demonstrate the asymptotic behavior of the solution. When $b/a = 1$, the results are those given for a circular pipe; however, when $a \to \infty$ the data differs from those given for a parallel plate channel.

8. Conclusion

The data presented here are taken from solutions of the Graetz-type problem for different flow passages. Accurate evaluation of the thermally developing temperature in the passages is a demanding task. Indeed the effect of the porosity further complicates the numerical evaluations. The alternative analysis, presented here, improves numerical accuracy when x becomes small. There are two unique features that should be mentioned here. First, this alternative procedure equally applies to passages having various shapes. Second, one can write the solution in more generalized Green's function solution form to accommodate the effect of frictional heating using the procedure described earlier.

References

[1] M. Kaviany, Laminar flow through a porous channel bounded by isothermal parallel plates, Int. J. Heat Mass Transfer 28 (4) (1985) 851–858.

[2] K. Vafai, S. Kim, Forced convection in a channel filled with porous medium: an exact solution, ASME J. Heat Transfer 111 (4) (1989) 1103–1106.

[3] A. Amiri, K. Vafai, Analysis of dispersion effects and non-thermal equilibrium, non-Darcian, variable porosity incompressible flow through porous media, Int. J. Heat Mass Transfer 37 (6) (1994) 939–954.

[4] D.-Y. Lee, K. Vafai, Analytical characterization and conceptual assessment of solid and fluid temperature differentials in porous media, Int. J. Heat Mass Transfer 42 (3) (1999) 423–435.

[5] B. Alazmi, K. Vafai, Analysis of variants within the porous media transport models, ASME J. Heat Transfer 122 (2) (2000) 303–326.

[6] D.A. Nield, A. Bejan, Convection in Porous Media, second ed., Springer-Verlag, New York, 1999.

[7] K. Kaviany, Principles of Heat Transfer in Porous Media, Springer-Verlag, New York, 1991.

[8] K. Vafai (Ed.), Handbook of Porous Media, Marcel Dekker, New York, 2000.

[9] D. Angirasa, Forced convective heat transfer in metallic fibrous materials, ASME J. Heat Transfer 124 (4) (2002) 739–745.

[10] D.A. Nield, A.V. Kuznetsov, M. Xiong, Effect of local thermal non-equilibrium on thermally developing forced convection in a porous medium, Int. J. Heat Mass Transfer 45 (25) (2002) 4949–4955.

[11] J.V. Beck, K.D. Cole, A. Haji-Sheikh, B. Litkouhi, Heat Conduction Using Green's Functions, Hemisphere, Washington, DC, 1992.

[12] D.A. Nield, A.V. Kuznetsov, M. Xiong, Thermally developing forced convection in a porous medium: parallel plate channel with walls at uniform temperature, with axial conduction and viscous dissipation effects, Int. J. Heat Mass Transfer 46 (4) (2003) 643–651.

[13] D.A. Nield, A.V. Kuznetsov, M. Xiong, Thermally developing forced convection in a porous medium: circular ducts with walls at constant temperature, with longitudinal conduction and viscous dissipation effects, Transport Porous Media 53 (3) (2003) 331–345.

[14] N.W. McLachlan, Theory and Application of Mathieu Functions, Dover, New York, 1964.

[15] I.S. Gradshteyn, I.M. Ryzhik, Table of Integrals, Series, and Products, Academic Press, New York, 1980.

[16] S. Wolfram, The Mathematica Book, fourth ed., Cambridge University Press, Cambridge, UK, 1999.

[17] L.V. Kantorovich, V.I. Krylov, Approximate Methods of Higher Analysis, Wiley, New York, 1960.